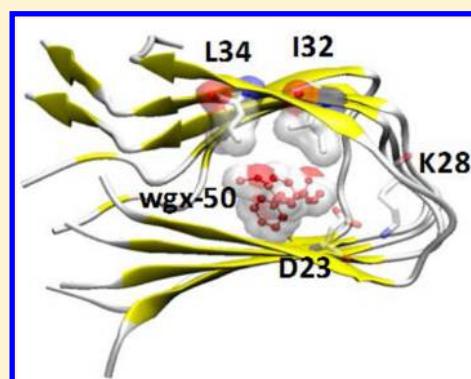


Destabilization of Alzheimer's A $\beta$ 42 Protofibrils with a Novel Drug Candidate wgx-50 by Molecular Dynamics SimulationsH.-M. Fu,<sup>†</sup> R.-X. Gu,<sup>†</sup> J. Wu,<sup>†</sup> L. Peng,<sup>†</sup> H. Li,<sup>‡</sup> Q. Xu,<sup>\*,†</sup>  
D.-Q. Wu<sup>\*,†</sup><sup>†</sup>State Key Laboratory of Microbial Metabolism and School of Life Science and Biotechnology, Shanghai Jiao Tong University, 800 Dongchuan Road, Shanghai 200240, China<sup>‡</sup>Medicine Engineering Research Center, School of Pharmacy, Chongqing Medical University, Chongqing 400016, China

## Supporting Information

**ABSTRACT:** Alzheimer's disease (AD) is one of the most common dementia. The aggregation and deposition of the amyloid- $\beta$  peptide (A $\beta$ ) in neural tissue is its characteristic symptom. To destabilize and dissolve A $\beta$  fibrils, a number of candidate molecules have been proposed. wgx-50 is a compound extracted from Sichuan pepper (*Zanthoxylum bungeanum*) and a potential candidate drug for treating AD. Our experimental results indicate that it is effective in destabilizing A $\beta$ 42 aggregation. A series of molecular dynamics simulation were performed in this work to explain the molecular mechanism of the destabilization of A $\beta$ 42 protofibrils by wgx-50. It is found that there are three possible binding sites including the hydrophobic groove on the surface of A $\beta$  protofibril that made no significant change in A $\beta$  structure and one site in the interior that caused destabilization of the protofibril. In this site, wgx-50 is packed against the side chain of I32 and L34, disrupted the D23–K28 salt bridge, and partially opened the tightly compacted  $\beta$ -sheet. The results were confirmed by simulation at 320 K, the deeper penetration of wgx-50 into the hole of protofibril is observed. The molecular mechanism of this novel drug candidate wgx-50 to disaggregate A $\beta$  protofibril may provide some insight into the treatment of tau-related dementia.



## INTRODUCTION

Abnormal aggregation of misfolded protein are associated with a number of fatal neurodegenerative diseases, including Alzheimer's disease (AD), Huntington's disease (HD), Parkinson's disease (PD), familial British dementia (FBD), familial Danish dementia (FDD), and type II diabetes.<sup>1–6</sup> In the elderly, AD is the most common dementia, with rapid increasing incidence and demand for treatment.<sup>7</sup> The pathological mechanism of AD is not fully understood; one of the major symptoms of AD is the presence of amyloid plaques in brain, which mainly consist of fibrils of the amyloid- $\beta$  peptide (A $\beta$ ).<sup>8</sup> The "amyloid hypothesis" suggested the aggregation and deposition of the A $\beta$  peptide in neural tissue to be the key of the AD.<sup>9</sup> Although the most toxic species of A $\beta$  is thought to be oligomers,<sup>10,11</sup> a series of studies also suggested possible contribution from oligomeric fibrils to the neurotoxicity in a mouse model.<sup>12–14</sup>

Various candidate targeting on A $\beta$  have been proposed, including antibodies, peptidic inhibitors, and nonpeptidic small molecules. For example, recent studies have suggested that some polyphenolic compounds from green tea may bind to A $\beta$ , inhibit A $\beta$  aggregation, and destabilize preformed fibrils.<sup>15,16</sup> In our previous work on the Alzheimer's mouse model found a novel lead of amyloid plaques and improved memory and cognitive ability after feeding of led

ine.<sup>17,18</sup> Encouraged by the excellent results, Rieker et al. proposed a hypothesis that the interaction between lead and A $\beta$  could shift the equilibrium of A $\beta$  polymorphism from  $\beta$ -sheet into disordered monomer.<sup>19</sup>

The advance in searching for A $\beta$  fibril's inhibitors are encouraging; however, the molecular detail of the interaction between the inhibitor and the A $\beta$  peptide are often unknown. This situation gradually changed by progress in investigation of the structure of A $\beta$  fibril, especially after a 3D structure was determined in 2005.<sup>20</sup> The unit of A $\beta$  fibril are generated by sequential cleavage of  $\beta$  and  $\gamma$  ectopeptides from the amyloid precursor protein (APP) into peptide of 40 or 42 amino acid, indicated by A $\beta$ 40 and A $\beta$ 42, respectively. Compared with A $\beta$ 40, A $\beta$ 42 has a stronger tendency to aggregate and comprise the dominant portion of A $\beta$  plaques in AD patients;<sup>21–24</sup> however, both of them may have a common structural motif of strand-loop-strand, which is aligned into two stacked  $\beta$ -sheet and further assembled into core- $\beta$  structure in the early hypothetical model.

**Special Issue:** Biman Bagchi Festschrift

**Received:** March 31, 2015

**Revised:** May 15, 2015

**Published:** May 21, 2015

The understanding in the context of  $A\beta$  fibril boosted the targeted design of inhibitory agents on them; however, partially due to the polymorphism of  $A\beta$  oligomers, their high-order polymers, many difficulties were encountered in the detailed molecular detail of the interaction between  $A\beta$  polypeptide and their inhibitors. One possible stabilization mechanism using traditional experimental method. On the contrary, computational method like molecular docking and molecular dynamics simulation exhibited attractive advantage and have been successively employed in the design of  $A\beta$  aggregation inhibitors in recent years. For example, using molecular dynamics simulation, Wand and co-workers characterized the binding site of a fluorescent dye, Thioflavin T (ThT), and its derivative on protofibrils of both  $A\beta_{9-40}$  and  $A\beta_{17-42}$ . A common binding motif consisting of groove formed by hydrophobic aromatic residue on the  $\beta$ -sheet surface along the fibril axis.<sup>25-27</sup> The Klimogroup studied anti-inflammatory agent, ibuprofen and naproxen, which may bind to the end of amyloid fibril to prevent fibril growth by a competitive mechanism, without significant change in the context of  $A\beta$  peptide.<sup>28-30</sup> Similarly, Lemke and Benington are mentioning the role of moxifloxacin, an effective antiaggregation flavonoid. It was found that moxifloxacin not only binds to the end of  $A\beta_{17-42}$  to block further combination of incoming peptide but also inserted into the hydrophobic core to disrupt intermolecular interaction like D23-K28 salt bridge and backbone hydrogen bond.<sup>31</sup>

In addition to the inhibitors above, N-[2-(3,4-dimethoxyphenyl)ethyl]-3-phenylacrylamide, also named g-50 (also called g-50), was designed by Wei et al.<sup>32</sup> and found in the extract of a natural flavonoid extract, *Sichuan pepper* (*Zanthoxylum Bungeanum*) (Figure 1). This novel design

candidate was suggested to possibly be an effective therapeutic agent for AD based on a series of biological experiments: in vitro experiments demonstrated that g-50 could disassemble  $A\beta$  oligomers, inhibit  $A\beta$ -induced neuronal apoptosis and apoptotic gene expression, and reduce neuronal calcium toxicity; in vivo experiments showed that g-50 could protect the blood brain barrier, decrease the accumulation of  $A\beta$  oligomers in the cerebral cortex, and improve the cognitive abilities of mice.<sup>33</sup> Found in natural food products, nontoxic in clinical studies and dose, capable of protecting the blood-brain barrier,<sup>17,18</sup> and effective in  $A\beta$  aggregation stabilization in vitro and in vivo, g-50 has many advantages to be an

attractive therapeutic candidate; however, the molecular mechanism for g-50 to destabilize the  $A\beta_{42}$  fibril is still unclear, which is to be studied in this ongoing molecular dynamics simulation, so that further targeted design and development could be applied to this type of inhibitory rational.

## METHODS

**Models of  $A\beta_{42}$  Protofibrils.** The model for simulation were constructed based on the solid-state NMR context of  $A\beta$  protofibril determined by Lühr et al. (PDB entry 2BEG).<sup>20</sup> Distinct from oligomeric species of  $A\beta$ , the pentameric context is a repeat unit of the mature  $A\beta$  fibril and is described as a protofibril of a core- $\beta$  sheet.<sup>34</sup> In this context, each peptide monomer has the disordered N-terminal residue 1-16 missing. The remaining residue 17-42 were suggested to contribute to the stability of the mature fibril model and were included in the simulation model here. This single core- $\beta$  sheet contains five identical peptide residues 17-42, labeled A-E (Figure 2), with a tail-loop tail motif,

connecting to interdigitated  $\beta$ -sheet hydrophobic chain zipper against each other in an antiparallel manner. In this unit, the direction of backbone hydrogen bond paralleled to the fibril axis, with the  $\beta$ -sheet perpendicular to it. Each U-helix peptide consists of an N-terminal  $\beta$ -sheet ( $\beta 1$ ) including residue V18-S26, a C-terminal  $\beta$ -sheet ( $\beta 2$ ) including residue I31-A42, and a loop (residue N27-A30) connecting them (Figure 2).

**MD Simulation Protocol.** All models of  $A\beta_{17-42}$  molecules with or without g-50 were modeled in a cubic box including about 11,000 atoms. Molecules more than 11 Å away from the model were deleted. The solvent water molecules were explicitly represented by the TIP3P model.<sup>35</sup> Five potassium ions ( $\text{K}^+$ ) were added to neutralize the net negative charge. Periodic boundary condition were applied in all directions. Following energy minimization, each of the temperature was simulated with positional restraints applied to peptide heavy atoms. With all of the positional restraints 14 Å of position-322.8 (see Table 1)

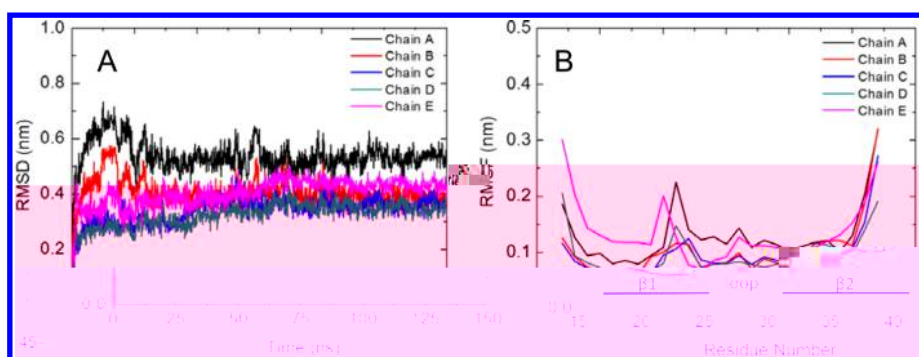


**Figure 3.** (A) Root-mean-square deviation (RMSD) and (B) root-mean-square fluctuation (RMSF) of the five chain during the simulation with  $A\beta$  protofibril alone. The color of the five chain is the same as the one in Fig. 2.

integration time step to 2 fs. The trajectory is saved every 10 ps for the following analysis. The hot-range and de Waal (VDW) interaction are treated using a 1.4 nm cutoff, and long-range electrostatic force are calculated by the Particle Mesh Ewald (PME) method.<sup>41</sup> The parameters of the g-50 molecule are from the AMBER GAFF parameter set.<sup>42</sup>

**Analysis Details.** Binding free energy are calculated using molecular mechanics/generalized Born surface area (MM-GBSA) in the AMBER package.<sup>43</sup> The global structural stability of the pentamer is measured by root-mean-square deviation (RMSD) of the backbone atoms with respect to initial minimized structure, while the root-mean-square atomic fluctuation (RMSF) are calculated for  $C\alpha$  atoms of each individual residue. The D23–K28 alt-bidge distance are calculated between the main center of the  $N\zeta$ -amino group and corresponding  $C\gamma$ -carbonyl. The average intrachain and interchain distance of  $\beta 1$  and  $\beta 2$  are calculated by the main center of the residue A21 and V36. The average interchain distance are calculated as the average distance of the main center of all the  $C\alpha$  atoms of neighboring chain. The hydrophobic interaction between g-50 and  $A\beta$  protofibril are evaluated by the number of hydrophobic contact, which is defined as a contact between a side chain carbon atom and a carbon atom in g-50 within a distance of 0.6 nm. The contact are visualized and figured by the VMD package.<sup>44</sup>

## RESULTS AND DISCUSSION

**Simulations of  $A\beta$  Protofibril Alone at 300 K.** Visual inspection of the 150 ns trajectory of the model for  $A\beta$  protofibril alone suggested that the overall  $A\beta$  structure is quite stable; only small deviation from the initial structure are observed. The major part of the  $\beta$ -strand are tightly packed to each other with tight dissociation, and the secondary structure of the strand-loop-strand motif is well-preserved. In the too open end of the  $\beta$ -strand, minor twisting made the five chain not entirely coplanar, optimized side-chain packing, hydrogen bond, and electrostatic interaction, and some that contributed to amorphous fibril stability as proposed previously<sup>45</sup> (Fig. S1 in the Supporting Information (SI)).

The overall structural stability of the fibril is measured by RMSD of the backbone atoms with respect to initial model of the minimized crystal structure. The five peptide chain are all generally stable, with the RMSD all are  $\sim 0.5$  nm, indicating a relatively low level of overall structural variation (Fig. 3A). From the RMSF profile (Fig. 3B), it is clear that this stability mainly comes from the too  $\beta$ -strand, where the hydrophobic

side chain of F19, A21, I32, L34, V36, and so on packed tightly. The most flexible region of each peptide are the residue at the N- and C-terminal, all the residue S26 and I31 connecting the  $\beta$ -strand and the loop. In this model, the terminal residue in the open end of  $\beta$ -strand are mostly exposed to the solvent and resulted in large fluctuation. Especially on the  $\beta 1$ -strand at C-terminal, the residue I41 and A42 beyond the  $\beta 2$ -strand at N-terminal are exposed and resulted in even higher flexibility. Another contribution to the overall stability of  $A\beta$  protofibril is the stabilization of the loop region by the interchain alt-bidge between residue D23 and K28, similar to many studies that suggested the importance of the D23–K28 alt-bidge.<sup>45,46</sup> Most of the D23–K28 alt-bidge are maintained during the hole simulation, with the average distance between the  $N\zeta$ -amino group and corresponding  $C\gamma$ -carbonyl being  $\sim 0.35 \pm 0.05$  nm.

**Binding of wgx-50 to  $A\beta$  Protofibril at 300 K.** The average period of 150 ns simulation of  $A\beta$  alone are repeated for 10 times at 300 K for the model of  $A\beta$  fibril with a g-50 molecule, in which three possible binding sites are found, however, sites A, B, and C (Fig. 4). Binding sites A and B

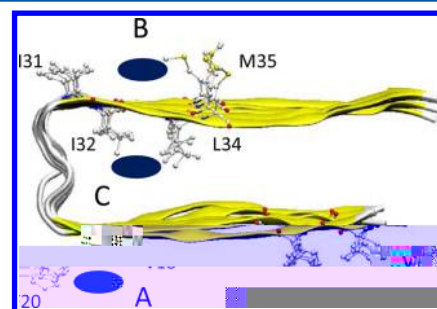


**Figure 4.** Three binding sites of g-50 on  $A\beta$  protofibril at 300 K: (A) V18–F20 groove on the surface of the  $\beta 1$  sheet. (B) I31–M35 groove on the surface of the  $\beta 2$  sheet. (C) Interdigitated site in the hydrophobic interface against the I32 and L34 side chain. For clarity, here the  $A\beta$  protofibril is simplified by the initial model, and the position of the three binding sites are indicated by blue ellipses.

residue in the V18–F20 groove on the surface of the  $\beta 1$  sheet and the I31–M35 groove on the surface of the  $\beta 2$  sheet, respectively (Fig. S2 in the SI). The electrostatic interaction between side chain of hydrophobic/aromatic residue, moreover, favorable for the hydrophobic g-50 to bind. Previous simulation also suggested that hydrophobic/aromatic and electrostatic interaction are stabilizing force for binding of residue

ligand.<sup>25</sup> Site C is in the interior of the pentameric  $A\beta$  fibril, between the side chain of I32 and L34 and the alt bridge between D23 and K28. All three binding sites of g-50 are also observed in peptide insertion on other  $A\beta$ -ligand complexes. Cook predicted the hydrophobic cleft between V18 and F20 as a plausible binding site for  $[R(bp)_2dppz]^{2+}$ .<sup>47</sup> Both sites on the surface were characterized in the binding of ThT and its derivative on  $A\beta$  fibril.<sup>25</sup> Partial insertion of monomer into the hydrophobic core was also founded in Lemkó's insertion.<sup>48</sup>

In the overall repeat of 150 ns MD simulation at 300 K and also at an elevated temperature 320 K a discrete, only binding to the three sites were observed to be stable enough to keep the ligand from escaping away. On the basis of MM/GBSA calculation, the insertion site has a binding energy of  $-35.5$  kcal/mol, which is much stronger than the  $-12.3$  kcal/mol of site A and  $-20.5$  kcal/mol of site B. The site is not guaranteed to be the only possible binding mode, but based on the results here, we would believe that this is the most possible one. In the following repeat of simulation at 300 K, one has g-50 stably bound at site A, one at site B, and two have it inserted into site C. The higher binding energy and the higher frequency to be observed in limited time of simulation may suggest the higher possibility for g-50 to be inserted into site C, and the influence of insertion to site C is also different with binding to site A or B. RMSD profiles suggest that the binding of g-50 to the sites A and B on the surface of the  $A\beta$  protofibril had little effect on its global stability, while the insertion into site C resulted in significant destabilization. (Figure S3 in the SI). Therefore, it is reasonable to assume that the possible role of g-50 in antiaggregation of  $A\beta$  fibril: (1) It binds to the top site on surface to hinder stacking of multiple units of the fibril into  $\alpha$ - $\beta$  complex and hence to ease aggregation; (2) it is inserted into the interior site C, causing significant deformation of the  $\alpha$ - $\beta$  bundle, and top assembly of the  $A\beta$  fibril.

It is interesting to notice that all three binding sites above were not predicted by a preliminary semiflexible docking using Autodock 4.2. When flexible g-50 was docked onto the rigid initial model of  $A\beta$  protofibril from the PDB structure 2BEG, the top predicted binding sites were mainly along the edge at chain A of the  $\alpha$ - $\beta$  bundle, relative to the binding site C, but in the initial model they were not enough space to accommodate the ligand. Therefore, it is impossible to find site C by docking it onto the rigid initial model. In MD simulation, the ligand was also observed to be temporarily associated with the site, but finally it gradually inserted into site C, with the separation of the interior space and partial deformation of the  $\alpha$ - $\beta$  bundle as described later. Although the groove at site A or B were not listed as top binding sites in docking, the binding energy could be enough for them to hold the ligand, in which need a conformational change and formation of a long hydrophobic interaction with surrounding residue may help to stabilize the bond state. The edict "induced fit" binding to the three sites were in MD simulation to describe the necessary conformational change in  $A\beta$  protofibril and could not be simply predicted by general semiflexible docking procedure using a rigid target. On the other hand, our MD protocol is equivalent to an iterative docking with flexible ligand considered for both the ligand and the target.

#### Destabilization of $A\beta$ Protofibril by wxg-50 Insertion.

In all simulation with g-50 inserted into the interior of  $A\beta$  protofibril, the entry of g-50 was always from the edge of

chain A, somewhat similar to the binding preference of ibuprofen to the concave (CV) edge simulated by Klimo et al.<sup>30</sup> In one simulation, g-50 was rapidly inserted into the hydrophobic interior of the  $A\beta$  protofibril within 40 ns, establishing a large number of hydrophobic contacts with side chain in the top  $\beta$ -sheet of the protofibril. The hydrophobic interaction might be the reason to allow the insertion of g-50 into the interior of  $A\beta$  protofibril, similar to the preferred binding to the hydrophobic groove of site A and B. The most important hydrophobic interaction is between the aromatic ring of g-50 and the side chain of I32 and L34 on chain A–C (Figure 5), which forced the lateral of  $\beta$  sheet

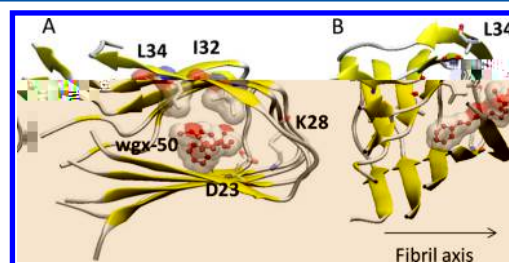


**Figure 5.** Insertion of g-50 into site C at 300 K shown by the final snapshot from top view (A) and alternative view (B). The packing of g-50 (in ball and stick) against the side chain of I32 and L34 (in tick) is visualized by surface rendering. The position of D23 and K28 are also indicated by tick.

to be contacted, and partially opened the tightly compacted structure of the  $\alpha$ - $\beta$  bundle. The compactness of the hydrophobic core comprising the  $\beta$ 2 portion of the fibril may be a crucial stabilization element in aggregation and elongation of  $A\beta$  aggregate.<sup>49,50</sup>

The partial opening of the  $\alpha$ - $\beta$  bundle by g-50 insertion destabilized the protofibril. The RMSD of the backbone atoms increased to almost 0.75 nm, suggesting an important destabilization of the  $A\beta$  protofibril. The RMSF of the residue were slightly increased, meaning higher flexibility of the chain after the g-50 insertion. This insertion also affected local conformation. The average distance between the charged moiety of the D23–K28 alt bridge were greater than 0.53 nm, far longer than the average of 0.35 nm in simulation of  $A\beta$  protofibril alone (Figure 6C). The integrity of the interchain alt bridge has been proposed to be an important contribution in the stability of the  $A\beta$  fibril, especially for the loop region.

In addition to co-rupture of the alt bridge, the number of the backbone hydrogen bond between chain A and chain B was also reduced to around 14 in the simulation after g-50 was inserted at site C, well below the control value of 19 hydrogen bonds in the simulation of  $A\beta$  protofibril alone (Figure S5 in the SI). The binding energy between chain A and chain B also decreased from  $-116.2$  to  $-104.5$  kcal/mol. The average interchain distance were calculated by the maximum of all the  $C\alpha$  atoms of each chain. The distance of  $A\beta$  protofibril alone is in good agreement with the experimental value  $0.48 \pm 0.05$  nm of the parallel  $\beta$ -sheet reported by Balbach et al.<sup>51</sup> At the same time,  $A\beta$  protofibril with g-50 inserted had this distance slightly increased to 0.53 nm, suggesting a tendency of detachment between the peptide. (Figure 6D)

The insertion of g-50 into site C caused contraction of the  $\alpha$ - $\beta$  bundle and dramatic rearrangement of top and  $\beta$ 1 and  $\beta$ 2. With g-50 inserted, the top  $\beta$ -strand of the same

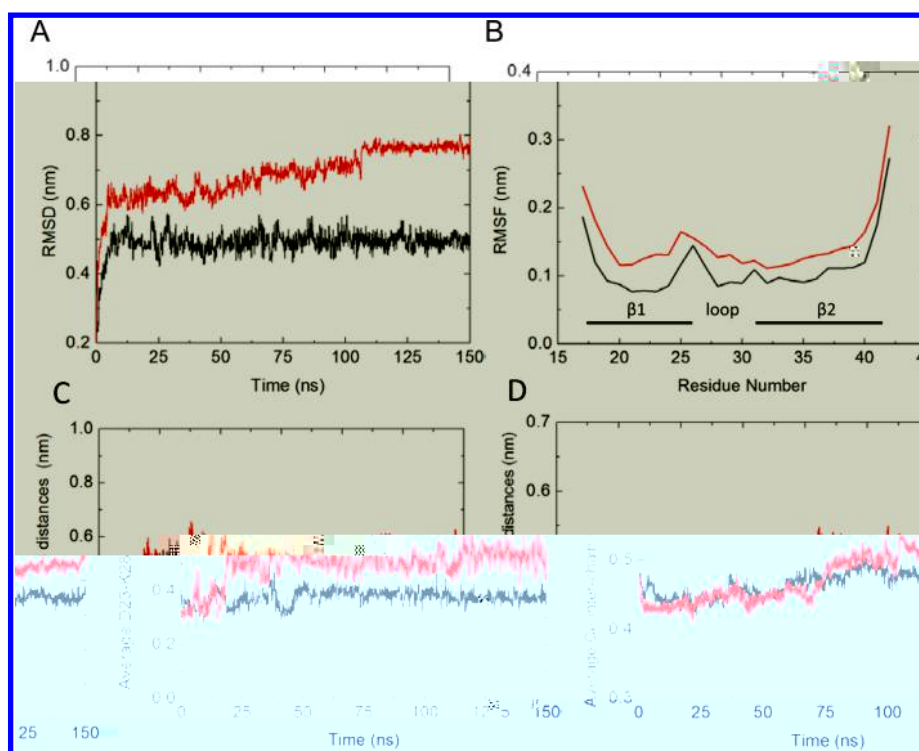


**Figure 6.** Destabilization of  $A\beta$  protofibril by  $wgx-50$  in solution at 300 K. (A) RMSD of the backbone atoms. (B) Root-mean-square fluctuation (RMSF). (C) D23–K28 distances between the main chain atoms of the N $\zeta$ -amino group and corresponding C $\gamma$ -carbonyl. (D) Average inter-chain distances between the main chain atoms of all the C $\alpha$  atoms of neighboring chains are compared between the simulation with  $A\beta$  protofibril alone (black) and with  $wgx-50$  in solution in the simulation (red).

chain significantly moved away from each other, resulting in a small translational shift between the two sheets and partial opening of the U-shaped structure of the  $\beta$ -strand and loop- $\beta$ -strand motif, especially at the chain A, B, and C (Figure 5). The loss of hydrophobic contact between A21 and V36 is observed by calculating the distance between the centers of mass of A21 and V36. All inter-chain distances between A21 and V36 increased overall. In particular, between chain A and B and between chain B and C, the distances were increased by 0.42 and 0.70 nm, respectively (Figure 7). Also, the average inter-chain A21–V36 distance was increased by 0.31 nm compared with the model of  $A\beta$  alone. (Figure S4 in the SI) The variation in the A21–V36 distance are observed

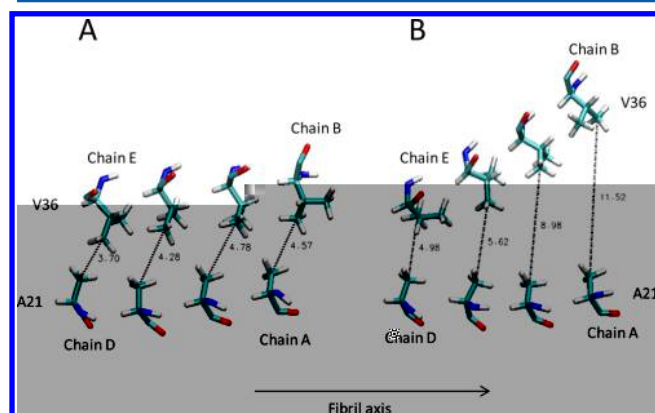


**Figure 7.** Reorganization of the  $\beta 1$  and  $\beta 2$  strands indicated by the increased inter-chain distances of A21 and V36 in the final snapshot of the simulation of  $A\beta$  protofibril alone (A) and with  $wgx-50$  in solution at 300 K (B) from the same time to Figure 5B.

indications of the rearrangement of the parallel, interdigitated, tightly compacted  $\beta$ -strand and loop- $\beta$ -strand motif, which are the basis of a core- $\beta$  sheet,<sup>52</sup> and a possible binding intermediate of  $A\beta$  fibril elongation.<sup>53</sup>

#### Simulations of $A\beta$ Protofibril with $wgx-50$ at 320 K.

The simulation of  $A\beta$  protofibril with  $wgx-50$  was repeated at 320 K, slightly elevated from 300 K to compare the influence of temperature on hydrophobic interaction. The results were similar to those at 300 K. The only difference was that the  $wgx-50$  penetrated more deeply into the hydrophobic interface of  $A\beta$  protofibril and packed against the side chain of I32 and L34 of chain A, B, C, and chain D (Figure S6A in the SI). The inter-chain A21–V36 distance was also increased. Different from the simulation at 300 K, the A21–V36 distance of chain C–D and chain D–E also increased significantly due to the deeper penetration (Figure 8).

As previously suggested, the hydrophobic interaction is a possible major contribution for the binding of  $wgx-50$  to  $A\beta$  protofibril. Thus, the number of hydrophobic contacts between  $wgx-50$  and  $A\beta$  protofibril were compared between the in solution simulation at 300 and 320 K. As shown in (Figure S6B in the SI), the number of atomic contacts between the peptide and  $wgx-50$  increased to the maximum number within the first 5 ns at 320 K, much faster than in the simulation at 300 K, where it took 45 ns to reach the maximum and became stable. Because the  $wgx-50$  is inserted into the hydrophobic core deeper at 320 K, the total number of hydrophobic contacts was generally 100 higher than in the simulation at 300 K.

## CONCLUSIONS

In this work, the binding of  $wgx-50$  onto  $A\beta$  protofibril is simulated by molecular dynamics simulation, where the destabi-

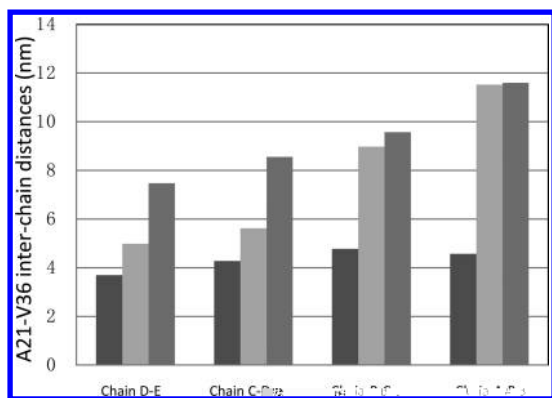


**Figure 8.** Average A21–V36 inter-chain distance in simulation of A $\beta$  peptide alone (dark gray) and with g-50 in the hole (light gray) at 300 K (left) and at 320 K (right).

lization of the peptide alone and its molecular mechanism was studied. Repeat of 150 ns MD simulation found the possible stable binding site, in which the hydrophobic groove on the surface of A $\beta$  peptide and one amino acid in the interior. Only insertion of g-50 into the interior could lead to significant destabilization of the peptide. The aromatic ring of g-50 was packed against the side chain of I32 and L34, partially disrupted the D23–K28 salt bridge critical to stabilize the loop region, and extended the distance of A21–V36, which are characteristic of the stacked  $\beta$ -strand-loop- $\beta$ -strand motif. The conformation of the parallel  $\beta$ -sheet and the partial opening of the too tightly compacted  $\beta$ -sheet of the core  $\beta$ -sheet destabilized the interaction between the peptide: the number of inter-chain backbone hydrogen bonds decreased, the average distance between the peptide chain was enlarged, and the inter-chain binding energy was lowered. The results were confirmed by simulation repeated at 320 K, the deeper insertion of g-50 into the hole peptide alone. The molecular dynamic simulation of g-50 to destabilize the A $\beta$  peptide alone may provide some insight into the mechanism of this novel drug candidate to disaggregate A $\beta$  fibrils and give some hint on the strategy of therapeutic drug design for AD.

## ASSOCIATED CONTENT

### Supporting Information

Final snapshot of the simulation of A $\beta$  peptide alone at 300 K from residue 1, binding of g-50 at site A from the side chain of  $\beta$ 1 sheet and at site B from the side chain of  $\beta$ 2 sheet, RMSD of the backbone atom in all simulation at 300 K, average inter-chain A21–V36 distance in the simulation of A $\beta$  alone and with g-50 in the hole at 300 K, number of the backbone hydrogen bond between chain A and chain B in the simulation of A $\beta$  alone and with g-50 in the hole at 300 K, insertion of g-50 into the interior of A $\beta$  peptide alone at 320 K, and comparison of the number of hydrophobic interaction between g-50 and the A $\beta$  peptide during the simulation with g-50 in the hole at 300 and 320 K. The Supporting Information is available free of charge on the ACS Publications website at DOI: 10.1021/acs.jpcc.5b03116.

## AUTHOR INFORMATION

### Corresponding Authors

\*Q.X.: E-mail: qin523@jtu.edu.cn

\*D.-Q.W.: E-mail: dawei@jtu.edu.cn.

### Notes

The authors declare no competing financial interest.

## ACKNOWLEDGMENTS

D.-Q.W. is supported by grant from the National High-Tech R&D Program (863 Program Contract No. 2012AA020307), the National Basic Research Program of China (973 Program) (Contract No. 2012CB721000), the Key Project of Shanghai Science and Technology Commission (Contract No. 11JC1406400), and Ph.D. Program Foundation of Ministry of Education of China (Contract No., 20120073110057). Q.X. is supported by grant from National Natural Science Foundation of China for Young Scholars (Grant No. 31400704).

## REFERENCES

- Temple, P. A.; Maino, L.; Pattoe, A. F. *Alzheimer's Disease: A Systematic Review of the Literature*. *EMBO J.* **2003**, *22* (3), 355–361.
- Cohen, F. E.; Kelly, J. W. The Amyloid Precursor Protein Folding Disease. *Nature* **2003**, *426* (6968), 905–909.
- Dobson, C. M. Protein Folding and Misfolding. *Nature* **2003**, *426* (6968), 884–890.
- Chiti, F.; Dobson, C. M. Protein Misfolding, Functional Amyloid, and Human Disease. *Annu. Rev. Biochem.* **2006**, *75*, 333–66.
- DeToma, A. S.; Salamekh, S.; Ramamoothy, A.; Lim, M. H. Misfolded Protein in Alzheimer's Disease and Type II Diabetes. *Chem. Soc. Rev.* **2012**, *41* (2), 608–621.
- Eisenberg, D.; Jucker, M. The Amyloid State of Protein in Human Disease. *Cell* **2012**, *148* (6), 1188–1203.
- Goedert, M.; Spillantini, M. G. A Century of Alzheimer's Disease. *Science* **2006**, *314* (5800), 777–781.
- Mononego, A.; Zota, V.; Kani, A.; Kiege, J. I.; Ba-O, A.; Bitan, G.; Bondan, A. E.; Selkoe, D. J.; Weine, H. L. Increased T Cell Reactivity to Amyloid Beta Protein in Old Human and Patient with Alzheimer's Disease. *J. Clin. Invest.* **2003**, *112* (3), 415–422.
- Hardy, J. A.; Higgins, G. A. Alzheimer's Disease: The Amyloid Cascade Hypothesis. *Science* **1992**, *256* (5054), 184–185.
- Kaede, R.; Head, E.; Thompson, J. L.; McIntire, T. M.; Milton, S. C.; Cotman, C. W.; Glabe, C. G. Common Structure of Soluble Amyloid Oligomers Implies Common Mechanism of Pathogenesis. *Science* **2003**, *300* (5618), 486–489.
- Leone, S.; Koh, M. T.; Kotilinek, L.; Kaede, R.; Glabe, C. G.; Yang, A.; Gallagher, M.; Ashe, K. H. A Specific Amyloid-Beta Protein Affects the Brain Impairment. *Nature* **2006**, *440* (7082), 352–357.
- Tai, J.; Gwendle, J.; Duff, K.; Gan, W. B. Fibrillar Amyloid Deposition Leads to Local Synaptic Abnormalities and Breakage of Neuronal Branches. *Nat. Neurosci.* **2004**, *7* (11), 1181–1183.
- Dehpande, A.; Mina, E.; Glabe, C.; Bioglio, J. Different Conformation of Amyloid Beta Induce Neurotoxicity by Distinct Mechanisms in Human Cortical Neurons. *J. Neurosci.* **2006**, *26* (22), 6011–6018.
- Picone, P.; Calotta, R.; Montana, G.; Nobile, M. R.; San Biagio, P. L.; Di Carlo, M. Abeta Oligomers and Fibrillar Aggregates Induce Different Apoptotic Pathways in LANS Neuroblastoma Cell Culture. *Biophys. J.* **2009**, *96* (10), 4200–4211.
- Ono, K.; Yoshiike, Y.; Takahima, A.; Hasegawa, K.; Naiki, H.; Yamada, M. Potent Anti-Amyloidogenic and Fibril-Destabilizing Effect of Polypheol in Vitro: Implication for Prevention and Therapeutic of Alzheimer's Disease. *J. Neurochem.* **2003**, *87* (1), 172–181.
- Hamaguchi, T.; Ono, K.; Yamada, M. Anti-Amyloidogenic Therapeutic Strategy for Prevention and Treatment of Alzheimer's Disease. *Cell. Mol. Life Sci.* **2006**, *63* (13), 1538–1552.

- (17) Ho, L.; Chen, L. H.; Wang, J.; Zhao, W.; Talcott, S. T.; Ono, K.; Teplo, D.; H mala, N.; Cheng, A.; Pe ci al, S. S.; et al. Hete ogeneity in Red Wine Polyphenolic Content Differentially Influence Alzheimer's Disease-Tyrosine Neurodegeneration and Cognitive Deterioration. *J. Alzheimer's Dis.* **2009**, *16* (1), 59–72.
- (18) Wang, J.; Ho, L.; Zhao, W.; Ono, K.; Ro en eig, C.; Chen, L.; H mala, N.; Teplo, D. B.; Pa inetti, G. M. G.ape-De.i ed Polyphenolic Peptide Abeta Oligomerization and Attenuate Cognitive Deterioration in a Mouse Model of Alzheimer's Disease. *J. Neurosci.* **2008**, *28* (25), 6388–6392.
- (19) Ri ie, C.; Dela na, J. C.; Immel, F.; C llin, C.; Monti, J. P. The Polyphenol Piceid Degrades Amyloid Fibril and Oligomer in Vitro: Hypothesis on Possible Molecular Mechanism. *Neurochem. Res.* **2009**, *34* (6), 1120–1128.
- (20) L h, T.; Ritte, C.; Ad ian, M.; Riek-Lohe, D.; Boh mann, B.; Doeli, H.; Sch be t, D.; Riek, R. 3D Structure of Alzheimer's Amyloid-Beta(1–42) Fibril. *Proc. Natl. Acad. Sci. U.S.A.* **2005**, *102* (48), 17342–17347.
- (21) Haa, C.; Selkoe, D. J. Soluble Protein Oligomer in Neurodegeneration: Lesson from the Alzheimer's Amyloid Beta-Peptide. *Nat. Rev. Mol. Cell Biol.* **2007**, *8* (2), 101–112.
- (22) M cke, L.; Ma liah, E.; Y, G. Q.; Mallo, M.; Rocken tein, E. M.; Tat no, G.; H, K.; Kholodenko, D.; John on-Wood, K.; McConlog e, L. High-Resolution Electron Microscopy of a Beta(1–42) in Wild-Type Human Amyloid Protein Precipitate from Transgenic Mice: Synaptotagmin III is a Plaques Formation. *J. Neurosci.* **2000**, *20* (11), 4050–4058.
- (23) Ja ett, J. T.; Lan b, P. T., J. Seeding “One-Dimensional Crystallization” of Amyloid: A Pathogenic Mechanism in Alzheimer's Disease and Scrapie? *Cell* **1993**, *73* (6), 1055–1058.
- (24) Selkoe, D. J. Translating Cell Biology into Therapeutic Advances in Alzheimer's Disease. *Nature* **1999**, *399* (6738), A23–A31.
- (25) W, C.; Bo e, M. T.; Shea, J.-E. On the Origin of the Stomach Binding of PIB or Thioflavin T to Protofibril of the Alzheimer's Amyloid-Beta Peptide: A Molecular Dynamic Study. *Biophys. J.* **2011**, *100* (5), 1316–1324.
- (26) W, C.; Scott, J.; Shea, J.-E. Binding of Congo Red to Amyloid Protofibril of the Alzheimer's A beta(9–40) Peptide Probed by Molecular Dynamic Simulation. *Biophys. J.* **2012**, *103* (3), 550–557.
- (27) W, C.; Wang, Z.; Lei, H.; Dan, Y.; Bo e, M. T.; Shea, J.-E. The Binding of Thioflavin T and Its Neutral Analog BTA-1 to Protofibril of the Alzheimer's Disease A beta(16–22) Peptide Probed by Molecular Dynamic Simulation. *J. Mol. Biol.* **2008**, *384* (3), 718–729.
- (28) Raman, E. P.; Takeda, T.; Klimo, D. K. Molecular Dynamic Simulation of IAPP Binding to Abeta Peptide. *Biophys. J.* **2009**, *97* (7), 2070–9.
- (29) Takeda, T.; K ma, R.; Raman, E. P.; Klimo, D. K. Nonsteroidal Anti-Inflammatory Drug Naproxen Degrades Amyloid Fibril: A Molecular Dynamic Investigation. *J. Phys. Chem. B* **2010**, *114* (46), 15394–402.
- (30) Chang, W. E.; Takeda, T.; Raman, E. P.; Klimo, D. K. Molecular Dynamic Simulation of Anti-Aggregation Effect of IAPP. *Biophys. J.* **2010**, *98* (11), 2662–2670.
- (31) Lemk l, J. A.; Be an, D. R. Degrading Alzheimer's Amyloid(42) Protofibril with Molecular Mechanism in Light of Molecular Dynamic Simulation. *Biochemistry* **2010**, *49* (18), 3935–3946.
- (32) G, R. X.; G, H.; Xie, Z. Y.; Wang, J. F.; A ia, H. R.; Wei, D. Q.; Cho, K. C. Possible Drug Candidate for Alzheimer's Disease Derived from Studying Their Binding Interaction with Alpha7 Nicotinic Acetylcholine Receptor. *Med. Chem.* **2009**, *5* (3), 250–262.
- (33) Tang, M.; Wang, Z.; Zho, Y.; X, W.; Li, S.; Wang, L.; Wei, D.; Qiao, Z. A Novel Drug Candidate for Alzheimer's Disease Treatment: G-50 Derived from Zanthoxylum Bungeanum. *J. Alzheimer's Dis.* **2013**, *34* (1), 203–213.
- (34) Shea, J. E.; U banc, B. Insight into Amyloid Aggregation: A Molecular Dynamic Perspective. *Curr. Top. Med. Chem.* **2012**, *12* (22), 2596–2610.
- (35) Jo gen en, W. L.; Chand a ekha, J.; Mad a, J. D.; Impe, R. W.; Klein, M. L. Comparison of Simple Potential Function for Simulating Liquid Water. *J. Chem. Phys.* **1983**, *79* (2), 926–935.
- (36) Van de Spoel, D.; Lindahl, E.; He, B.; G oenhof, G.; Ma k, A. E.; Be end en, H. J. C. GROMACS: Fast, Flexible, and Free. *J. Comput. Chem.* **2005**, *26* (16), 1701–1718.
- (37) Dan, Y.; W, C.; Cho dh, S.; Lee, M. C.; Xiong, G. M.; Zhang, W.; Yang, R.; Cieplak, P.; Lo, R.; Lee, T.; et al. A Point-Charge Force Field for Molecular Mechanics Simulation of Protein Based on Condensed-Phase Quantum Mechanical Calculation. *J. Comput. Chem.* **2003**, *24* (16), 1999–2012.
- (38) Ho nak, V.; Abel, R.; Ok, A.; St ockbine, B.; Roitbe g, A.; Simme ling, C. Comparison of Multiple Amber Force Field and Development of Improved Protein Backbone Parameters. *Proteins* **2006**, *65* (3), 712–725.
- (39) Be end en, H. J. C.; Po tma, J. P. M.; an G n te en, W. F.; DiNola, A.; Haak, J. R. Molecular Dynamics with Coupling to an External Bath. *J. Chem. Phys.* **1984**, *81* (8), 3684–3690.
- (40) He, B.; Bekke, H.; Be end en, H. J. C.; Fa aije, J. LINCS: A Linear Constraint Solver for Molecular Simulation. *J. Comput. Chem.* **1997**, *18* (12), 1463–1472.
- (41) Da den, T.; Yo k, D.; Pede en, L. Particle Mesh Ewald: an  $N \log(N)$  Method for Ewald Summation in Large Systems. *J. Chem. Phys.* **1993**, *98* (12), 10089–10092.
- (42) Wang, J. M.; Wolf, R. M.; Cald ell, J. W.; Kollman, P. A.; Ca e, D. A. Development and Testing of a General Amber Force Field. *J. Comput. Chem.* **2004**, *25* (9), 1157–1174.
- (43) Kollman, P. A.; Ma o a, I.; Re e, C.; K hn, B.; Ho, S.; Chong, L.; Lee, M.; Lee, T.; Dan, Y.; W, W.; et al. Calculating Structure and Free Energy of Complex Molecule: Combining Molecular Mechanics and Continuum Model. *Acc. Chem. Res.* **2000**, *33*, 889–897.
- (44) H mph e, W.; Dalke, A.; Sch lten, K. VMD: Visual Molecular Dynamics. *J. Mol. Graphics Modell.* **1996**, *14* (1), 33–38.
- (45) Zheng, J.; Jang, H.; Ma, B.; Tai, C.-J.; N i no, R. Modeling the Alzheimer's A beta(17–42) Fibril Architecture: Tight Intermolecular Sheet-Sheet Association and Intermolecular Hydrogen Bonding. *Biophys. J.* **2007**, *93* (9), 3046–3057.
- (46) Thi malai, D.; Klimo, D. K.; Dima, R. I. Emerging Idea on the Molecular Basis of Protein and Peptide Aggregation. *Curr. Opin. Struct. Biol.* **2003**, *13* (2), 146–159.
- (47) Cook, N. P.; O bil, M.; Kat ampe, C.; P abhaka, R.; Ma ti, A. A Unifying Photoluminescence Response of Light-Sensitive Rhodamine(II) Complexes Bound to Amyloid-Beta. *J. Am. Chem. Soc.* **2013**, *135* (29), 10810–10816.
- (48) A tie o, I.; Sa iano, M.; Langella, E. In Silico Investigation and Targeting of Amyloid Beta Oligomer of Different Size. *Mol. Biosyst.* **2013**, *9* (8), 2118–2124.
- (49) Ma man, M. F.; Ei el, U. L.; C i madia, I. G.; Penke, B.; En iz, R. D.; Ma ink, S. J.; L iten, P. G. In Silico Study of Full-Length Amyloid Beta 1–42 Tri- and Penta-Oligomer in Solution. *J. Phys. Chem. B* **2009**, *113* (34), 11710–11719.
- (50) B chete, N.-V.; H mme, G. Structure and Dynamics of Parallel Beta-Sheet, Hydrophobic Core, and Loop in Alzheimer's Amyloid Fibril. *Biophys. J.* **2007**, *92* (9), 3032–3039.
- (51) Balbach, J. J.; Petko a, A. T.; O le, N. A.; Ant r tkin, O. N.; Go don, D. J.; Me edith, S. C.; T cko, R. S. p amolecula Structure in Full-Length Alzheimer's Beta-Amyloid Fibril: Evidence for a Parallel Beta-Sheet Organization from Solid-State Nuclear Magnetic Resonance. *Biophys. J.* **2002**, *83* (2), 1205–1216.
- (52) Ki chne, D. A.; Ab aham, C.; Selkoe, D. J. X-Ray-Diffraction from Intermolecular Paired Helical Filament and Ectopic Amyloid Fibrils in Alzheimer's Disease Indicate Core-Beta Conformation. *Proc. Natl. Acad. Sci. U.S.A.* **1986**, *83* (2), 503–507.
- (53) Han, W.; W, Y. D. A Strand-Loop-Strand Structure in a Possible Intermediate in Fibril Elongation: Long Time Simulation of Amyloid-Beta Peptide (10–35). *J. Am. Chem. Soc.* **2005**, *127* (44), 15408–15416.